A COMPACT *H*-PLANE MAGIC TEE DESIGNED AT W BAND

Z. X. Wang, W. B. Dou, and Z. L. Mei [†]

State Key Lab of Millimeter waves
Southeast University
Nanjing 210096, P. R. China

Abstract—Magic tee is a widely used component in microwave systems; the four arms of a conventional magic tee direct at four different directions, which occupy much space and give inconveniences to the assemblage of a system. In this paper, a waveguide narrow-wall slot directional coupler and an *E*-plane dielectric loaded waveguide phase shifter are used to make up of a magic tee with four arms in the same *H*-plane. The narrow-wall slot directional coupler is analyzed with mode matching method and optimized with simulated annealing method, and the dielectric loaded waveguide phase shifter is designed with edge based finite element method. Numerical results of the magic tee are presented, which show that the performance of the designed magic tee is good.

1. INTRODUCTION

Magic tee is a widely used component in microwave systems and it can be used to make up of many functional components such as sum-and-difference network in a mono-pulse antenna system, frequency discriminator and balanced mixer, etc. Conventional magic tee is a matched waveguide double-tee, and the four arms locate in different planes (*E*-plane and *H*-plane), which makes the magic tees occupy much space and especially not suitable for planar circuits. As everyone knows, a $-3\,\text{dB}$ directional coupler combining with a $\pi/2$ phase shifter gives the performance of magic tee, so in this paper, a planar magic tee based on a $-3\,\text{dB}$ *H*-plane narrow-wall slot directional coupler (NWSDC) and a dielectric loaded rectangular waveguide phase shifter (DLWPS) is designed, and the four arms of this kind of magic tee

---

[†] Also with Guangzhou Haige Communications Group, Guangzhou, P. R. China

locate in the H-plane (called HPMT in the following). The NWSDC contains many slots and wall sections, and it is to say that different combination of the slots and wall sections gives a different NWSDC, so a large number of NWSDC based on different combination of the slots and wall sections should be simulated to find out the best one which realizes a -3 dB directional power, which is a time consuming course, and for this reason, fast computing method is needed to simulate the transmission characteristic of the NWSDC. On the other hand, to search the best combination of the slots and wall sections, a multi-parameters optimization method has to be used. So in this paper mode matching method (MMM) [1, 2] and the simulated annealing method (SAM) [3] are combined to design and optimize the NWSDC. Though MMM is efficient for designing the NWSDC, it is difficult to design the DLWPS using this method if the loaded dielectric block is irregular, so edge based finite element method (EBFEM) [4] is used to design and analyze the DLWPS. EBFEM not only has all the advantages of the traditional FEM, but also overcomes the drawback of pseudo-solution which is often met in the traditional FEM [5]. In Section 2, the design of the NWSDC using MMM combined with SAM is discussed; in Section 3, the design of the DLWPS using the EBFEM is introduced; then in Section 4, two HPMT examples are given and the scattering characteristics of the HPMT are presented.

2. DESIGN OF THE NWSDC

2.1. Theory

The structure of a NWSDC is shown in Fig. 1(a), the two waveguide are coupled through the slots in the narrow wall. The key to design the coupler is to obtain the width of the slots and the width of the walls between the slots.

See Fig. 1(b), the overall scattering matrix S_D of the NWSDC may be obtained by the direct combination of all the local scattering matrixes S_c^1, S_c^2, ..., S_c^N [6, 7]. According the odd and even mode incident wave theory [8], in order to solve the local scattering matrixes, say S_c^1, we may firstly solve a two-port scattering matrix $S^{2p}(e)$ of the hatched section (see Fig. 1(c)) in the case when $w(x = 0)$ is magnetic wall, and a two-port scattering matrix $S^{2p}(o)$ of the hatched section in the case when $w(x = 0)$ is electric wall, then the scattering matrixes
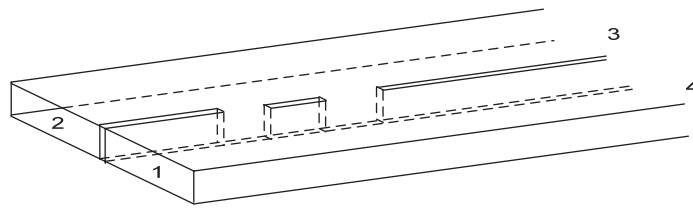
(a) Overall view
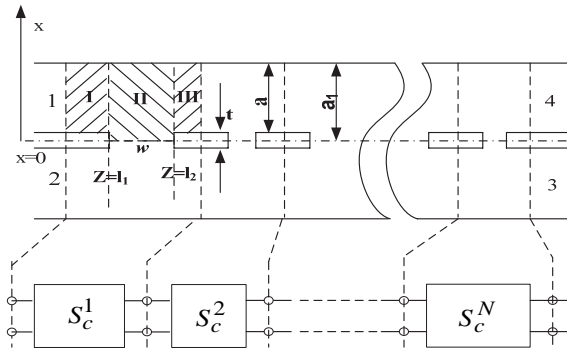
(b) Top view
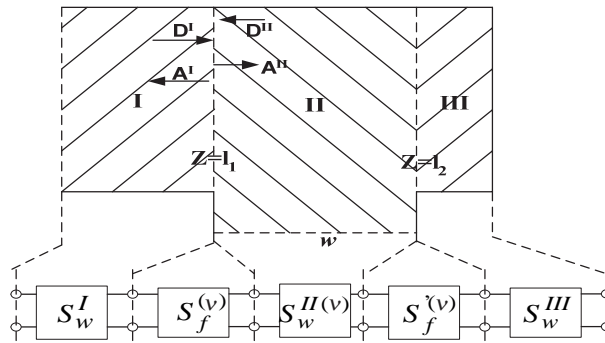
(c) Zoom-in view of the hatched section in (b)

Figure 1. Configuration of the narrow-wall slot directional coupler.

S_c^1 can be expressed as:

$$S_c^1 = \begin{bmatrix} (S_{11}^{c1}) & (S_{21}^{c1}) & (S_{31}^{c1}) & (S_{41}^{c1}) \\ (S_{21}^{c1}) & (S_{22}^{c1}) & (S_{32}^{c1}) & (S_{31}^{c1}) \\ (S_{31}^{c1}) & (S_{32}^{c1}) & (S_{22}^{c1}) & (S_{21}^{c1}) \\ (S_{41}^{c1}) & (S_{31}^{c1}) & (S_{21}^{c1}) & (S_{11}^{c1}) \end{bmatrix} \tag{1}$$

where

$$\left(S_{11}^{c1}\right) = \frac{1}{2}\left[\left(S_{11}^{2p}(e)\right) + \left(S_{11}^{2p}(o)\right)\right] \tag{2a}$$

$$\left(S_{21}^{c1}\right) = \frac{1}{2}\left[\left(S_{21}^{2p}(e)\right) + \left(S_{21}^{2p}(o)\right)\right] \tag{2b}$$

$$\left(S_{22}^{c1}\right) = \frac{1}{2}\left[\left(S_{22}^{2p}(e)\right) + \left(S_{22}^{2p}(o)\right)\right] \tag{2c}$$

$$\left(S_{31}^{c1}\right) = \frac{1}{2}\left[\left(S_{21}^{2p}(e)\right) - \left(S_{21}^{2p}(o)\right)\right] \tag{2d}$$

$$\left(S_{32}^{c1}\right) = \frac{1}{2}\left[\left(S_{22}^{2p}(e)\right) - \left(S_{22}^{2p}(o)\right)\right] \tag{2e}$$

$$\left(S_{41}^{c1}\right) = \frac{1}{2}\left[\left(S_{11}^{2p}(e)\right) - \left(S_{11}^{2p}(o)\right)\right] \tag{2f}$$

The two-port scattering matrix $S^{2p}(\nu)$ can be obtained by direct combination of five two-port scattering matrixes: S_w^I, S_f^ν, $S_w^{II(\nu)}$, $S_f'^\nu$ and S_w^{III} ($\nu = e$ or o when w is magnetic wall or electric wall respectively). S_w^I, $S_w^{II(\nu)}$ and S_w^{III} are the scattering matrix of the waveguide I, II and III respectively, S_f^ν is the scattering matrix of the discontinuity at $z = l_1$, and $S_f'^\nu$ is the scattering matrix of the discontinuity at $z = l_2$, however, $S_f'^\nu$ can be obtained directly from S_f^ν by exchanging the ports of the two-port scattering matrix. Considering the case when the incident wave is TE_{10} mode, the waves excited in region I can be expressed as

$$\begin{cases} E_{yn}^I = \sum_{n=1}^{N}\left(A_n^I e^{jk_{zn}^I z} + D_n^I e^{-jk_{zn}^I z}\right)\sin k_{xn}\left(x - t/2\right) \\ H_{xn}^I = \sum_{n=1}^{N}\frac{k_{zn}^I}{w\mu}\left(A_n^I e^{jk_{zn}^I z} - D_n^I e^{-jk_{zn}^I z}\right)\sin k_{xn}\left(x - t/2\right) \end{cases} \tag{3}$$

where

$$k_{xn}^I = n\pi/a.$$
$$k_{zn}^I = \sqrt{k_0^2 - (k_{xn}^I)^2}.$$

A_n^I and D_n^I represent the amplitudes of the scattering wave and the incident wave in region I.

The waves excited in region II can be expressed as

$$\begin{cases} E_{yn}^{II} = \sum_{n=1}^{N} \left(A_n^{II} e^{-jk_{zn}^{II}z} + D_n^{II} e^{jk_{zn}^{II}z} \right) \sin k_{xn}^{II} x \\ H_{xn}^{II} = \sum_{n=1}^{N} \frac{k_{zn}^{II}}{w\mu} \left(-A_n^{II} e^{-jk_{zn}^{II}z} + D_n^{II} e^{jk_{zn}^{II}z} \right) \sin k_{xn}^{II} x \end{cases} \quad (4)$$

where $k_{xn}^{II} = n\pi/a_1$, when w is electric wall, or $k_{xn}^{II} = (2n+1)\pi/(2a_1)$, when w is magnetic wall.

$$k_{zn}^{II} = \sqrt{k_0^2 - (k_{xn}^{II})^2}.$$

The continuous conditions at the interface $z = l_1$ are

$$\begin{cases} E_y^I = E_y^{II} \mid_{z=l_1} & t/2 \leq x \leq a_1 \\ E_y^{II} = 0 & x \leq t/2 \end{cases} \quad (5a)$$

$$H_x^I = H_x^{II} \mid_{z=l_1} \qquad t/2 \leq x \leq a_1 \quad (5b)$$

Matching the tangential field component [9, 10] at $z = l_1$ according to (5a) and (5b), the coefficients A_n^I and A_n^{II} can be related to each other by a group of equations, solving these equations to get A_n^I and A_n^{II}, and then S_f^ν can be written as

$$S_f^\nu = \begin{bmatrix} \left(A^I(I) \right) & \left(A^I(II) \right) \\ \left(A^{II}(I) \right) & \left(A^{II}(II) \right) \end{bmatrix} \quad (6)$$

where $\left(A^I(II) \right)$ is the coefficient matrix of the scattering wave in region I when incident by $\left(D^{II} \right)$, and other symbols can be understood similarly.

The scattering matrix of waveguide I, II and III can be easily obtained, and can be written as

$$S_w^p = Diag \left\{ e^{-jk_{zn}^p L} \right\} p = I, \ II \text{ or } III. \quad (7)$$

As there are many slots and wall sections in the NWSDC, the SAM is used to find the optimized combination of the sizes of the slots and wall sections.

2.2. Numerical Results

Based on the theory described in 2.1, a-3 dB NWSDC using eight slots is designed at w band with the width of waveguide $a = 2.54$ mm, the configuration ($d1 = d8 = 1.41$ mm, $d2 = d7 = 0.3$ mm, $d3 = d6 = 1.58$ mm, $d4 = d5 = 1.46$ mm, $t = 0.6$ mm, $L1 = L7 = 0.77$ mm, $L2 = L6 = 2.25$ mm, $L3 = L5 = 1.22$ mm, $L4 = 1.49$ mm) and its scattering parameters are shown in Fig. 2. The NWSDC is also computed using HFSS 9.0, and the results agree well with that obtained by MMM in this paper (see Fig. 2(b)).
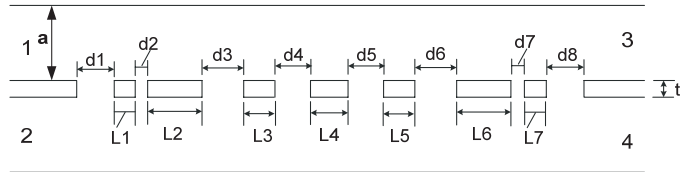
(a) Top view
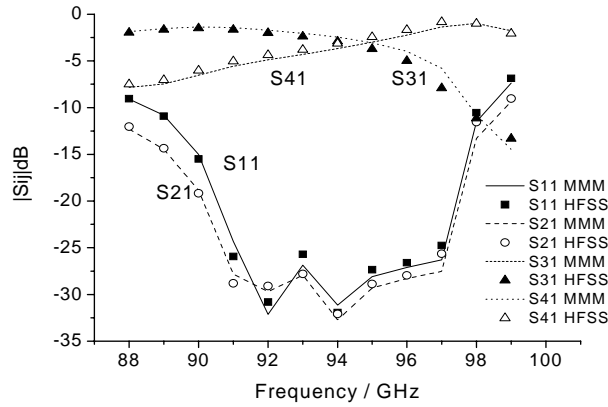
(b) Scattering parameters

Figure 2. Configuration of the eight-slot narrow-wall directional coupler and its scattering parameters.

In order to design a NWSDC with better performance, more slots have to be used, and this means more parameters may be used in the optimization procedure, which will add difficulties to the designing. Heinz Schmiedel and Fritz Arndt have given a solution in [11], where they tandem connect two -8.34 dB directional coupler to get a -3 dB directional coupler. This solution is adopted in this paper. We designed a -8.34 dB NWSDC using six slots first (the scattering

parameter is shown in Fig. 3(a)), then connect two such directional couplers to get a -3 dB directional coupler (twelve slots), and the scattering parameter of the -3 dB NWSDC is shown in Fig. 3(b). It can be seen that the reflection of port 1 and the isolation between port 1 and port 2 is less than -30 dB in a wide bandwidth of 6 GHz (from 91 GHz to 97 GHz).
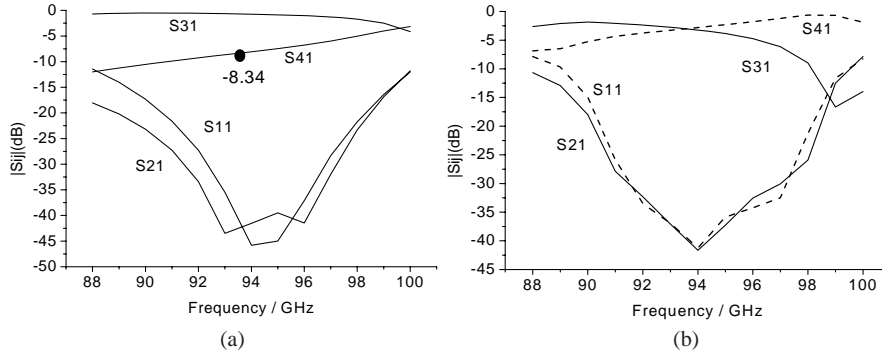

Figure 3. (a) S-parameters of the -8.34 dB NWSDC using six slots, (b) S-parameters of the -3 dB NWSDC constructed by two -8.34 dB NWSDCs.

3. DESIGN OF THE DLWPS

In this paper, dielectric is loaded to the waveguide to achieve a phase shift of $\pi/2$, as the dielectric block may be irregular, and it is difficult to analyze it with MMM, so the EBFEM is used to analyze and design the phase shifter.

3.1. Theory of the EBFEM for Solving General Scattering Parameters of Waveguide Discontinuity Problems

A typical waveguide discontinuity problem is shown in Fig. 4, the electric field $\vec{E}$ in the region V enclosed by the port face S_1, S_2 and the conductor boundary satisfies

$$\nabla \times \left(\frac{1}{\mu_r} \nabla \times E \right) - k^2 \varepsilon_r E = 0 \tag{8}$$

Assume the incident wave of unit amplitude transmits along z direction, then the total field at the port face S_1 can be expressed by
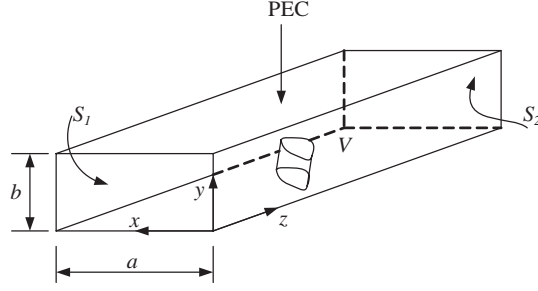
Figure 4. Waveguide loaded with dielectric block.

the sum of the incident field and the scattered field [4], and the electric field can be expressed as

$$E(x, y, z) = \sum_{m=0}^{\infty} \sum_{n=0}^{\infty} a_{mn} \vec{e}_{mn}^{TE}(x, y) e^{\gamma_{mn} z}$$
$$+ \sum_{m=1}^{\infty} \sum_{n=1}^{\infty} b_{mn} \left[\vec{e}_{tmn}^{TM}(x, y) + \hat{z} \vec{e}_{zmn}^{TM} x, y) \right] e^{\gamma_{mn} z} \quad (9)$$

At the port face S_2 the scattered electric field can be expressed by

$$E(x, y, z) = \sum_{m=0}^{\infty} \sum_{n=0}^{\infty} c_{mn} \vec{e}_{mn}^{TE}(x, y) e^{-\gamma_{mn} z}$$
$$+ \sum_{m=1}^{\infty} \sum_{n=1}^{\infty} d_{mn} \left[\vec{e}_{tmn}^{TM}(x, y) - \hat{z} \vec{e}_{zmn}^{TM}(x, y) \right] e^{-\gamma_{mn} z} \quad (10)$$

where

$$\vec{e}_{mn}^{TE}(x, y) = N_{mn} \left(\hat{x} \frac{n}{b} \cos \frac{m\pi x}{a} \sin \frac{n\pi y}{b} - \hat{y} \frac{m}{a} \sin \frac{m\pi x}{a} \cos \frac{n\pi y}{b} \right) \ (11)$$

$$\vec{e}_{tmn}^{TM}(x, y) = N_{mn} \left(\hat{x} \frac{m}{a} \cos \frac{m\pi x}{a} \sin \frac{n\pi y}{b} + \hat{y} \frac{n}{b} \sin \frac{m\pi x}{a} \cos \frac{n\pi y}{b} \right) \ (12)$$

$$\vec{e}_{zmn}^{TM}(x, y) = \frac{N_{mn}}{\pi \gamma_{mn}} \left[\left(\frac{m\pi}{a} \right)^2 + \left(\frac{n\pi}{b} \right)^2 \right] \sin \frac{m\pi x}{a} \sin \frac{n\pi y}{b} \qquad (13)$$

$$N_{mn} = \sqrt{\nu_m \nu_n} \bigg/ \sqrt{n^2 \frac{a}{b} + m^2 \frac{b}{a}}, \quad \nu_m = \begin{cases} 1 & m = 0 \\ 2 & m \neq 0 \end{cases} \ (14)$$

In expression (9) and (10), a_{mn}, b_{mn}, c_{mn}, d_{mn} are unknown constant coefficients; a_{mn} and b_m represent the reflection coefficient of

the mn-th TE mode and the mn-th TM mode at S_1 respectively; c_{mn} and d_{mn} represent the transmission coefficient of the mn-th TE mode and the mn-th TM mode at S_2 respectively. Discretize the region V with tetrahedron elements and set up the FEM linear equations set as that in [4], the electric field at S_1 and S_2 can be calculated, then the coefficients a_{mn}, b_{mn}, c_{mn} and d_{mn} can be determined by

$$a_{mn} = e^{-\gamma_{mn}z_1} \int_0^a \int_0^b \vec{e}_{mn}^{TE} \cdot \left[\vec{E} - \vec{E}^{inc}\right]_{z=z_1} dxdy \tag{15}$$

$$b_{mn} = e^{-\gamma_{mn}z_1} \int_0^a \int_0^b \vec{e}_{tmn}^{TM} \cdot \left[\vec{E} - \vec{E}^{inc}\right]_{z=z_1} dxdy \tag{16}$$

$$c_{mn} = e^{\gamma_{mn}z_2} \int_0^a \int_0^b \vec{e}_{mn}^{TE} \cdot \vec{E}|_{z=z_2} dxdy \tag{17}$$

$$d_{mn} = e^{\gamma_{mn}z_2} \int_0^a \int_0^b \vec{e}_{tmn}^{TE} \cdot \vec{E}|_{z=z_2} dxdy \tag{18}$$

After a_{mn}, b_{mn}, c_{mn} and d_{mn} are obtained, the general scattering parameter of the DLWPS can be given directly as

$$S = \begin{bmatrix} (a_{mn}, b_{mn}) & (c_{mn}, d_{mn}) \\ (c_{mn}, d_{mn}) & (a_{mn}, b_{mn}) \end{bmatrix} \tag{19}$$

For the H-plane problem, expression (19) can be simplified as

$$S = \begin{bmatrix} (a_{mn}) & (c_{mn}) \\ (c_{mn}) & (d_{mn}) \end{bmatrix} \tag{20}$$

3.2. Numerical Results of the Designed DLWPS

The EBFEM was implemented with C program language; then the scattered parameters of unmatched double tee was calculated to testify our program, numerical results obtained by our program agree well with the results in [12], see Fig. 5.

Then the program was used to design the DLWPS. In order to realize the characteristic of the magic tee, the phase of the transmitted wave at the exit port of the DLWPS should be $\pi/2$ ahead of the standard waveguide. Assuming the transmitting coefficient of the DLWPS is S_{21}^p, and the transmitting coefficient of the standard waveguide is S_{43}^w (see Fig. 6(a)), then the following relation should be satisfied,

$$re\left(S_{21}^p\right) - im\left(S_{43}^w\right) = 0, \quad im\left(S_{21}^p\right) + re\left(S_{43}^w\right) = 0 \tag{21}$$

(a)   (b)
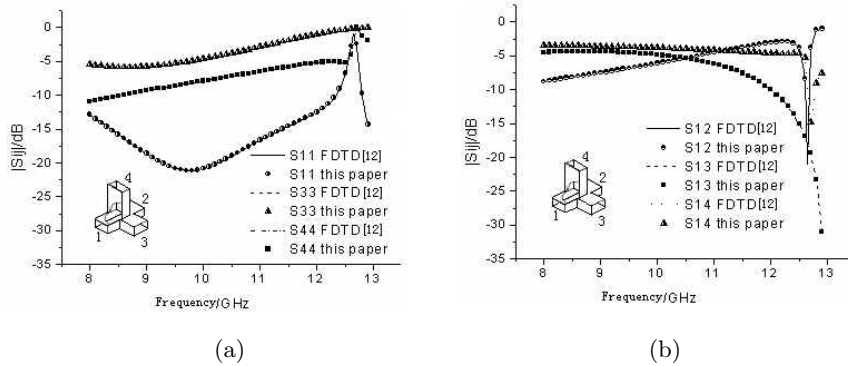
Figure 5. Scattering parameters of the unmatched tee.

where $re\left(S_{21}^{p}\right)$ and $im\left(S_{21}^{p}\right)$ are the real part and imaginary part of S_{21}^{p} respectively, $re\left(S_{43}^{w}\right)$ and $im\left(S_{43}^{w}\right)$ are the real part and imaginary part of S_{43}^{w} respectively.

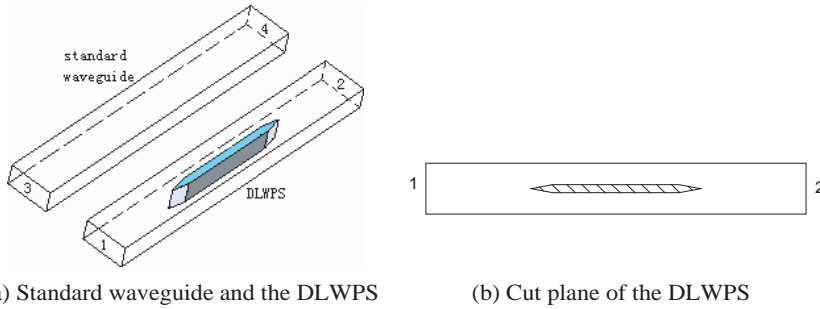(a) Standard waveguide and the DLWPS   (b) Cut plane of the DLWPS

Figure 6. Designed DLWPS.

A designed DLWPS is shown in Fig. 6. The DLWPS is realized by waveguide loaded with dielectric slab which is full height and has wedge-shaped end and front; the characteristic of the DLWPS is shown in Fig. 7, both the scattering characteristic and the phase shifting characteristic are very good.

4. CHARACTERISTIC OF THE MAGIC TEE

After the S-parameter of the NWSDC (S_{D}), S-parameter of the DLWSP (S_{DLWSP}) and S-parameter of the standard waveguide (S_{SW}) are obtained, the S-parameter of the HPMT can be obtained by direct

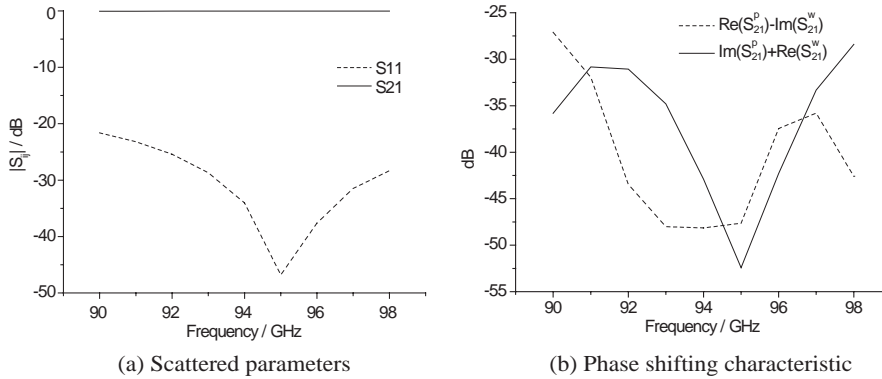(a) Scattered parameters   (b) Phase shifting characteristic

Figure 7. Characteristic of the DLWPS.

combination of these three S-parameter matrixes, and the sketch map of the matrix combination is shown in Fig. 8.
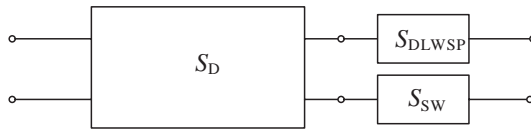

Figure 8. S-parameter matrix combination sketch.

In a $-3\,\mathrm{dB}$ NWSDC, the phase of the output wave from port 3 leads $\pi/2$ phase ahead of port 4 when incident at port 1. If a phase shifter is linked to port 3 and a waveguide of the same length is linked to the port 4, when the phase shifter leads $\pi/2$ phase ahead of the waveguide, the output wave from port 3 leads π phase ahead of that from port 4, and this gives the performance of a magic tee. Two HPMT have been designed using eight-slot and twelve-slot NWSDC respectively with the DLWSP. The configuration of the twelve-slot HPMT is shown in Fig. 9, and configuration of the eight-slot HPMT is similar. Numerical results of the two HPMT are given in Fig. 10 and Fig. 11. The reflection and isolation of the twelve-slot HPMT (see
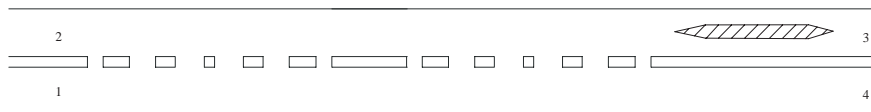

Figure 9. Configuration of the twelve-slot HPMT.

Fig. 11(a)) is nearly $-30\,\text{dB}$ in a frequency band of $7\,\text{GHz}$, which is better than that of the eight-slot HPMT (see Fig. 10(a)). When TE_{10} mode is incident at port 1, output waves of port 3 and port 4 should be out phase and carry equal power, this could be represented by the following expression:
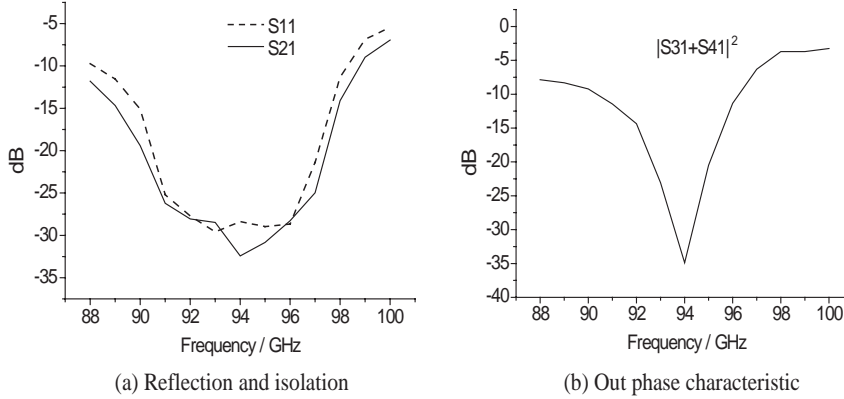
$$|S31 + S41| \to 0 \qquad\qquad (22)$$

Figure 10. Characteristic curves of the eight-slot HPMT.

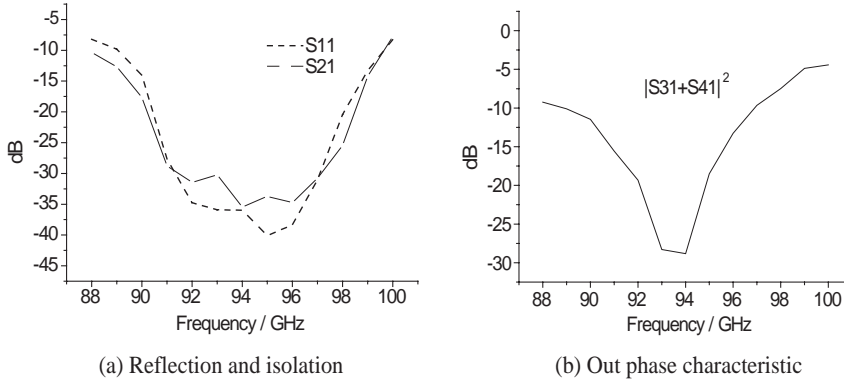(a) Reflection and isolation   (b) Out phase characteristic

Figure 11. Characteristic curves of the twelve-slot HPMT.

The numerical results of $|S31 + S41|$ are shown in Fig. 10(b) and Fig. 11(b) in dB form for the two HPMT respectively. The $-20\,\text{dB}$ bandwidth of the twelve-slot HPMT is nearly $3\,\text{GHz}$, better than that of the eight-slot HPMT (only $2\,\text{GHz}$).

5. CONCLUSION

In this paper, two NWSDCs are designed using MMM combined with the SAM and a DLWPS is designed using EBFEM, then by combination of the DLWPS with the NWSDCs respectively, two HPMTs are presented. With the four arms located in the same H-plane, it is convenient for this kind of magic tee to be used in planar circuits and be assembled in a system. Numerical analysis shows that the presented HPMTs have good performances.

REFERENCES

1. Riabi, M. L., R. Thabet, and M. Belmeguenai, "Rigorous design and efficient optimizattion of quarter-wave transformers in metallic circular waveguides using the mode-matching method and the genetic algorithm," *Progress In Electromagnetics Research*, PIER 68, 15–33, 2007.
2. Huang, R. and D. Zhang, "Application of mode matching method to analysis of axisymmetric coaxial discontinuity structures used in permeability and/or permittivity measurement," *Progress In Electromagnetics Research*, PIER 67, 205–230, 2007.
3. Press, W. H., S. A. Teukolsky, W. T. Vetterling, and B. P. Flannery, *Numerical Recipes in C*, 2nd edition, Cambridge University Press, 1995.
4. Jin, J. M., *The Finite-element Method in Electromagnetics*, John Wileys & Sons, Inc., New York, 1993.
5. Hernandez-Lopez, M. A. and M. Quintillan-Gonzalez, "A finite element method code to analyse waveguide dispersion," *Journal of Electromagnetic Waves and Applications*, Vol. 21, No. 3, 397–408, 2007.
6. Arndt, F., B. Koch, H.-J. Orlok, and N. Schroder, "Field theory design of rectangular waveguide broad-wall metal-insert slot couplers for millimeter-wave applications," *IEEE Trans. on Microwave Theory and Techniques*, Vol. 33, No. 2, 95–104, 1985.
7. Partzelt, H. and F. Arndt, "Double-plane steps in rectangular waveguides and their application for transformers, irises, and filters," *IEEE Trans. on Microwave Theory and Techniques*, Vol. 30, No. 5, 771–776, 1982.
8. Reed, J. and G. J. Wheeler, "A method of analysis of symmetrical four-port networks," *IRE Trans. Microwave Theory Tech.*, Vol. 4, 246–252, 1956.

9. Uher, J., J. Bornemann, and U. Rosenberg, *Waveguide Components for Antenna Feed Systems: Theory and CAD*, Artech House Publishers, May 1, 1993.

10. Park, J. K., D. H. Shin, J. N. Lee, and H. J. Eom, "A full-wave analysis of a coaxial waveguide slot bridge using the Fourier transform technique," *Journal of Electromagnetic Waves and Applications*, Vol. 20, No. 2, 143–158, 2006.

11. Schmiedel, H. and F. Arndt, "Field theory design of rectangular waveguide multiple-slot narrow-wall couplers," *IEEE Trans. on Microwave Theory and Techniques*, Vol. 34, No. 7, 791–797, 1986.

12. Ritter, J. and F. Arndt, "Efficient FDTD/matrix-pencil method for the full-wave scattering parameter analysis of waveguiding structures," *IEEE Trans. on Microwave Theory and Techniques*, Vol. 44, No. 12, 2450–2456, 1996.